ACS OMEGA

http://pubs.acs.org/journal/acsodf

Article

Azelaic Acid/Expanded Graphite Composites with High Latent Heat Storage Capacity and Thermal Conductivity at Medium Temperature

Giang Tien Nguyen, Ha Soo Hwang, Jiyoung Lee, and In Park*

Cite This: *ACS Omega* 2021, 6, 8469−8476

Read Online

ACCESS | Metrics & More | Article Recommendations

ABSTRACT: A novel azelaic acid/expanded graphite (AA/EG) phase change composite (PCC) was fabricated as a shape-stabilized phase change material (PCM) for latent heat storage at medium temperatures. The composite exhibited a low supercooling degree and high heat storage capacity. Despite the impregnation of a high quantity of AA (85 wt %) in the porous network of EG, there was no leakage of liquid AA. This was attributed to the capillary forces and surface tension forces. The pure AA exhibited a melting temperature of 108.0 °C, with an intrinsically low supercooling degree of 5.8 °C. The melting temperature of AA in the PCC decreased slightly to 105.8 °C, and there was a significant decrease in the supercooling degree to 1.0 °C. The AA/EG PCC exhibited a high latent heat storage capacity of 162.5 J/g, and there was a significant gap between the decomposition temperature and the phase change temperature range. Therefore, the composite exhibited high thermal stability during operations. The results of an accelerated thermal cycling test (200 cycles) indicated the high cycling durability and chemical stability of the PCC. The thermal conductivity of AA increased by 15.7 times after impregnation in EG, as compared to that of the pure AA, and thus, thermal kinetics of the PCC was improved. The results of a heat storage/release test with 15 g of the PCM revealed that the melting and solidification of the AA/EG PCC were 5.0-fold and 7.4-fold faster, respectively, than those of the pure AA. This was attributed to the high thermal conductivity of the PCC.

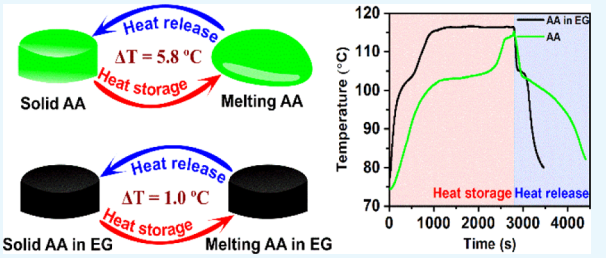

1. INTRODUCTION

Thermal energy storage (TES) is an important strategy for the efficient utilization of thermal energy to alleviate the issue of fossil fuel shortage.[1] Latent heat storage (LHS), among the various TES technologies, has attracted significant attention owing to the high energy storage capacity for LHS systems; furthermore, the heat storage/release in such systems occurs at a defined temperature that corresponds to the phase change temperature.[2] The energy storage capacity for LHS systems is 5−14-fold higher than that for sensible heat storage systems at the same unit volume.[3] Phase change materials (PCMs) are employed as the storage media in LHS systems. The application of PCMs in the low-temperature range (T < 80 °C) has been extensively researched, and PCMs are commercially utilized worldwide for low-temperature applications. The application of PCMs in the medium-temperature region (80 °C < T < 250 °C) remains relatively unexplored despite its immense economic potential.[4] It has been determined that up to 5−6% of the annual energy consumption in Germany occurs at 100−300 °C. The thermal energy in this temperature range is utilized not only for steam generation, hot/cold conditioning, and cooking but also in the textile, paper, and rubber industries.[5] Recently, there has been significant interest in the working of PCMs at 100−130 °C for solar energy applications.[6,7]

The utilization of organic and inorganic PCMs for medium-temperature applications presents different advantages and disadvantages.[6,8] The optimal PCMs should be nontoxic, noncorrosive, and abundantly available; additionally, they should exhibit a high heat storage density, high cycling durability, and a low supercooling degree.[9] Hydroxides, nitrates, carbonates, and their eutectics are classified as inorganic PCMs.[5] They are thermally stable and inexpensive; however, their applications are limited by drawbacks such as inhomogeneous melting, phase separation, and corrosion.[4]

Organic PCMs usually exhibit homogeneous melting, no phase separation, and little or no corrosion,[2] unlike the inorganic PCMs. However, the supercooling degree, which is defined as the difference between the melting and crystallization temperatures, of organic PCMs is high. Although most

Received: January 15, 2021
Accepted: March 2, 2021
Published: March 16, 2021

sugar alcohols (galactitol, mannitol, and erythritol) exhibit ultrahigh heat storage capacity, their applicability is hindered by the undesirably high supercooling degrees of up to 65 °C.[10,11] Salicylic acid, benzanilide, and hydroquinone also exhibit high supercooling degrees of 13−48 °C.[12] A eutectic mixture of adipic acid and sebacic acid exhibits a supercooling degree of 17 °C.[13] The optimal supercooling degree of a PCM should be less than 5 °C.[14] The addition of nucleating agents such as silver iodide (AgI), calcium pyrophosphate ($Ca_2P_2O_7$), aluminum phosphate ($AlPO_4$), and graphite foam reportedly alleviates the drawback of the high supercooling degree.[15] However, the combination with nucleating agents lowers the heat storage density of PCMs. This is attributed to not only the replacement of the PCM by the nucleating agents but also the unexpected interactions between the PCM and additives. The addition of only 6.5% of graphite foam induced a 13% decrease in the heat storage density of a eutectic mixture of galactitol and mannitol.[15] It is preferable to utilize materials with inherently low supercooling degrees so that no additional effort is required to lower the supercooling degree.

The applications of PCMs are also limited by issues such as low thermal conductivity and pronounced liquid leakage, in addition to the high supercooling degree.[16] A widely used technique for the alleviation of these drawbacks is the impregnation of PCMs in porous matrixes to form phase change composites (PCCs).[17] The impregnated PCMs are confined in the pores of the matrixes by the capillary and surface tension forces, thereby preventing the leakage of the liquid PCMs.[18,19] Silica-based materials, such as silica gel[20] and silica fume,[21] carbon-based materials, such as expanded graphite (EG)[6,8,22] and carbon nanotube (CNT) sponge,[23] and silicate minerals, such as expanded perlite[24] and vermiculite,[25] are utilized as the supporting materials for PCCs. The lightweight and inexpensive EG is a promising supporting material owing to its high porosity, which ensures a high PCM content in the porous support and high thermal conductivity. Xia et al.[26] demonstrated that the impregnation of 93 wt % of paraffin in only 7 wt % of EG induced a significant increase (10 times) in the thermal conductivity of paraffin. Wang et al.[27] demonstrated the excellent shape stabilization of a sebacic acid/EG composite that was prepared with 85 wt % of the PCM. The thermal conductivity of the composite was 5.35 W/m·K, whereas that of pure sebacic acid was only 0.37 W/m·K. These results indicated the efficacy of EG as a porous support for medium-temperature PCMs.

Azelaic acid [$HOOC(CH_2)_7COOH$] (AA) is a dicarboxylic acid that is naturally found in wheat and barley. It is nonhazardous and suitable for cost-effective large-scale production. It is utilized in the medicine and polymer industries.[28,29] AA has been utilized as a PCM in only one study (1996)[30] to the best of our knowledge. The phase change temperature of AA was determined to be ∼107 °C, which is suitable for medium-temperature applications. However, the other thermal properties of AA such as the LHS capacity, supercooling degree, thermal stability, and cycling durability have not been investigated. AA exhibits a high LHS capacity (∼202 J/g) and a relatively low supercooling degree (5.8 °C). Therefore, it is necessary to conduct an in-depth evaluation of the suitability of AA as a medium-temperature PCM.

A series of novel AA/EG PCCs was prepared for medium-temperature applications in the present study. AA was impregnated into the porous network of EG via evaporative impregnation. The optimal content of AA (85 wt %) in the pores of EG was determined by the leakage tests. The confinement of AA in the pores of EG lowered the supercooling degree of AA. The Fourier-transform infrared (FT-IR) spectra and X-ray diffraction (XRD) patterns for AA and the 85 wt % AA/EG PCC revealed the absence of chemical interactions between AA and the EG surface. The cycling durability was investigated over 200 accelerated thermal cycles to determine the chemical and physical stability of the PCC. The thermal conductivity of the PCC increased by 15.7 times as compared to that of the pure AA. The heat storage/release behaviors were investigated using a homemade apparatus. The melting and solidification rates of the PCC (15 g) were 5.0-fold and 7.4-fold higher, respectively, than those of the pure AA (15 g) (75 → 120 → 75 °C).

2. RESULTS AND DISCUSSION

2.1. Characterization of the AA/EG PCCs. Figure 1 shows the scanning electron microscopy (SEM) images of EG and the AA/EG PCCs. EG is a widely utilized porous support, and its porosity has been investigated in detail in other studies.[26,27,31,32] The EG particles (Figure 1a) exhibited a worm-like structure, while the pores of EG (Figure 1b) were crevice-like; furthermore, net-like pores were formed by the graphite flakes. These pores consisted primarily of mesopores and macropores, and the largest pores reached sizes of several microns. The presence of pores resulted in a high pore volume that facilitated the impregnation of the PCM into the pores. The SEM images of the AA/EG PCCs with different AA contents are presented in Figure 1c−f. The edge of the EG layers remained vacant for the composites with AA contents of 80 wt % (Figure 1c) and 85 wt % (Figure 1d). However, it was

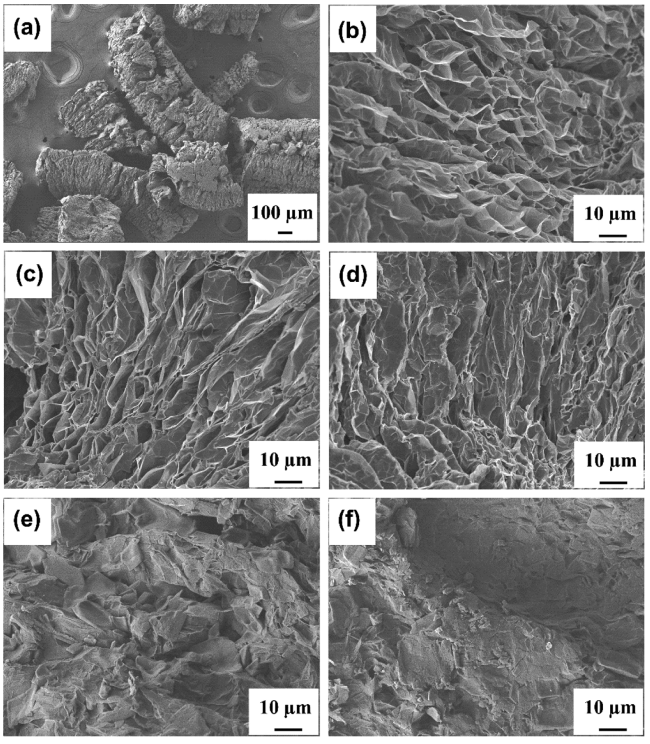

Figure 1. SEM images of (a) EG (50×), (b) EG (1000×), and AA/EG PCCs with different AA contents; (c) 80 wt % (1000×), (d) 85 wt % (1000×), (e) 90 wt % (1000×), and (f) 95 wt % (1000×).

https://dx.doi.org/10.1021/acsomega.1c00265
ACS Omega 2021, 6, 8469−8476

filled with an increasing amount of bulk AA with the increase in the AA content to 90 wt % (Figure 1e) and 95 wt % (Figure 1f). Consequently, an excessive quantity of AA was present in the 90 and 95 wt % AA/EG PCCs.

A leakage test was performed to investigate the shape stability of the AA/EG PCCs. The composites with various AA contents (80−95 wt %) were initially collected on filter papers; subsequently, they were placed in an oven at 130 °C (~20 °C higher than the melting point of AA) for 60 min. Thereafter, the composites were removed from the filter papers and observed to detect the stains of AA (Figure 2). The amount of

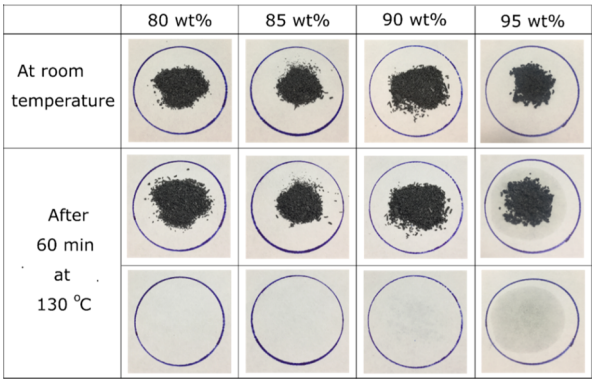

Figure 2. Optical microscopy images of the AA/EG PCCs with various AA contents during the leakage test.

the leaked AA from the 95 wt % AA/EG PCC was markedly high, whereas that from the 90 wt % AA/EG PCC was negligible. The 80 and 85 wt % AA/EG PCCs exhibited no leakage of AA, which indicated their excellent shape stability. EG effectively confined ~85 wt % of AA via the capillary forces and surface tension forces, thereby preventing the leakage. These results were consistent with the other reports, where the maximum PCM content without leakage was determined to be 85−93 wt %.[18,26,27,31] The increase in the PCM content induced an increase in the TES capacity. Therefore, the composite with 85 wt % AA was selected as the optimal AA/EG PCC for further investigations. The subsequent results in this work will be discussed with respect to the 85 wt % AA/EG PCC.

The chemical compatibility of the AA/EG PCCs was investigated by FT-IR spectroscopy (Figure 3a). The FT-IR spectrum of the pure EG exhibited a broad band that was centered at 3409 cm^{-1}. This band was assigned to the −OH stretching mode from either the alcoholic/phenolic functional groups of EG or the surface-adsorbed water.[33,34] The peak at 1619 cm^{-1} was assigned to the C−O vibration mode. The broad peak within 3700−2300 cm^{-1} in the FT-IR spectrum of AA corresponded to the stretching vibrations of the −OH groups. The peaks at 2931 and 2854 cm^{-1} were assigned to the stretching vibrations of the −C−H bonds. The peaks at 1697, 1419, 1311, and 910 cm^{-1} were assigned to the stretching vibrations of the C═O groups, the bending vibration of the −C−H bonds, stretching vibrations of the C−O groups, and the bending mode of the −OH groups, respectively. The characteristic peaks of AA overlapped with those of EG in the FT-IR spectrum of the AA/EG PCC. Moreover, no new peaks were detected. This indicated the physical compounding of EG and AA without the occurrence of chemical reactions. Therefore, EG and AA exhibited high chemical compatibility in the PCC.

The crystallographic properties of EG, AA, and the 85 wt % AA/EG PCC were characterized by XRD (Figure 3b). The XRD pattern for EG presented one high-intensity peak at 2θ = 26.6° that corresponded to the characteristic (002) peak of graphite. Figure 3b shows the XRD patterns of the two crystalline phases of AA, that is, the α- and β-forms.[35] The XRD pattern of the commercial form of AA (α) presented five high-intensity reflections that were centered at 2θ = 8.4, 19.0, 22.1, 23.5, and 28.2°. The α-form of AA transformed to the β-form after melting and recrystallization. The XRD pattern for β-form AA presented five peaks at 2θ = 9.4, 18.6, 19.2, 23.0, and 27.2°. The XRD pattern for the 85 wt % AA/EG PCC exhibited all the characteristic peaks of EG and β-form AA. This was attributed to the melting and recrystallization of AA in the pores of EG during the preparation of the PCC. The low intensity of the peak at 9.4° was attributed to contrast matching between EG and the confined AA in the pore.[36] The absence of new peaks in the pattern indicated the physical combination of EG and AA without the occurrence of chemical reactions.

2.2. Phase Change Properties of the AA/EG PCC. The phase change properties of the pure AA and the 85 wt % AA/EG PCC were investigated using differential scanning calorimetry (DSC) (Figure 4). The melting/solidifying temperatures (T_M/T_S), melting/solidifying enthalpies ($\Delta H_M/\Delta H_S$) (LHS capacities), and supercooling degrees ($\Delta T = T_M -$

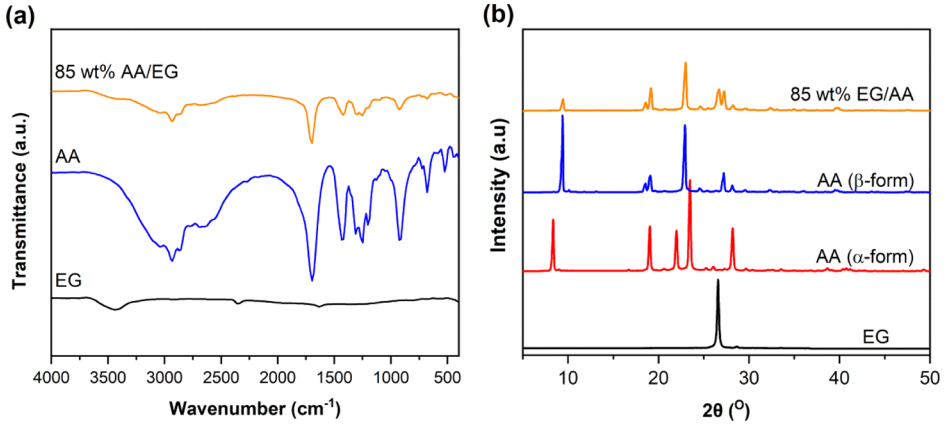

Figure 3. (a) FT-IR spectra and (b) XRD patterns of EG, AA, and the 85 wt % AA/EG PCC.

https://dx.doi.org/10.1021/acsomega.1c00265
ACS Omega 2021, 6, 8469−8476

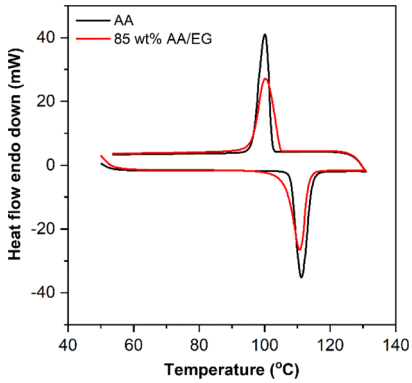

Figure 4. DSC curves of the pure AA and the 85 wt % AA/EG PCC.

T_S) are presented in Table 1. An endothermic peak and an exothermic peak were presented during melting and solidification, respectively, by both the pure AA and the PCC. The T_M and T_S of the pure AA were 108.0 and 102.2 °C, respectively; thus, the pure AA exhibited a relatively low supercooling degree (ΔT) of 5.8 °C. The PCC exhibited a lower T_M (105.8 °C) and a higher T_S (104.8 °C) as compared to those exhibited by the pure AA. Thus, the supercooling degree of the PCC (1.0 °C) was lower than that of the pure AA. This was attributed to the fact that the inner surface of EG functioned as a heterogeneous nucleation center to not only accelerate the crystallization but also decrease the particle size of AA during the crystallization.[31,37]

Table 1. Phase Change Properties of the Pure AA and the 85 wt % AA/EG PCC

	T_M (°C)	ΔH_M (J/g)	T_S (°C)	ΔH_S (J/g)	ΔT (°C)	F (%)
AA	108.0	202.0	102.2	201.2	5.8	100
85 wt % AA/EG	105.8	162.5	104.8	162.2	1.0	94.7
85 wt % AA/EG (after 200 thermal cycles)	105.9	158.4	105.0	158.0	0.9	92.3

The LHS capacities, that is, the ΔH_M and ΔH_S of the pure AA were 202.0 and 201.2 J/g, respectively. The ΔH_M and ΔH_S of the PCC were 162.5 and 162.2 J/g, respectively. The phase change latent heat of the PCC was lower than that of the pure AA owing to the presence of EG with no latent heat. The phase change latent heat might also have been lowered by the confinement effects that suppressed the crystallization of the confined PCM. The impact of the confinement on the crystallinity of the PCM was evaluated by calculating the crystallization fraction (F) using the following equation (eq 1)

$$F = \frac{(\Delta H_{M,PCC} + \Delta H_{S,PCC})}{(\Delta H_{M,PCM} + \Delta H_{S,PCM}) \times x} \times 100 \quad (1)$$

where $\Delta H_{M,PCC}$ and $\Delta H_{S,PCC}$ are the melting and solidifying enthalpies of the PCC, respectively, and x is the relative mass fraction of the PCM in the composite. The crystallization fraction of the 85 wt % AA/EG PCC was as high as 94.7%. The confinement of AA in the porous network of EG exerted a negligible effect on the crystallinity of AA. Therefore, the PCC retained a high crystallinity that optimized its LHS capacity.

The melting LHS capacity (ΔH_M) and the supercooling degree (ΔT) of the 85 wt % AA/EG PCC were compared to those of the other medium-temperature PCCs in the previous studies (Table 2). The ΔH_M and ΔT of the 85 wt % AA/EG PCC were higher and lower, respectively, than those of [$LiNO_3$–$NaNO_3$–KNO_3–$Ca(NO_3)_2$]/calcium silicate, [$Ca(NO_3)_2$–$NaNO_3$]/EG, [KNO_3–$LiNO_3$–$Ca(NO_3)_2$–$CsNO_3$]/EG, and ($NaNO_3$–KNO_3)/EG. The ΔH_M of the 85 wt % AA/EG PCC was lower than that of erythritol/EG and erythritol–mannitol/EG. However, the ΔT of the 85 wt % AA/EG PCC was significantly lower than that of erythritol/EG and erythritol–mannitol/EG. The ΔH_M and ΔT of the 85 wt % AA/EG PCC were comparable to those of sebacic acid/EG and sebacic acid/CNT sponge. The results indicated that the 85 wt % AA/EG PCC in the present study exhibited an optimal LHS capacity and supercooling degree.

2.3. Thermal Stability of the AA/EG PCC. The thermal stabilities of the pure AA and the AA/EG PCC were examined by thermogravimetric analysis (TGA) (Figure 5). The TGA curves at 400 °C revealed the approximately 100% weight loss for the pure AA. The 85 wt % AA/EG PCC exhibited a weight loss of 85.6%, which was similar to the AA content. AA was uniformly impregnated in the EG matrix. The pure AA exhibited onset and endset decomposition temperatures of 228–274 °C. The 85 wt % AA/EG PCC exhibited onset and endset decomposition temperatures of 256–321 °C. The higher thermal stability of the PCC as compared to that of the pure AA was attributed to the interactions, such as capillary forces and surface tension forces, between AA and the pore surfaces of EG.[36] Furthermore, the absence of decomposition at temperatures close to the phase change temperature of the

Table 2. Comparison of the ΔH_M, ΔT, and Thermal Conductivity Increment for the Medium-Temperature PCCs and the AA/EG PCC

PCCs	T_M (°C)	ΔH_M (J/g)	ΔT[a] (°C)	EG ratio (wt %)	thermal conductivity increment[b] (times)	(refs)
[$LiNO_3$–$NaNO_3$–KNO_3–$Ca(NO_3)_2$]/calcium silicate	103.5	73.6			2.5	38
[$Ca(NO_3)_2$–$NaNO_3$]/EG	216.8	89.8	6.1	7	7.3	8
[KNO_3–$LiNO_3$–$Ca(NO_3)_2$–$CsNO_3$]/EG	113.1	87.9		10	30	4
($NaNO_3$–KNO_3)/EG	220	109.0	3	20	7	22
erythritol/EG	106	212.5	19.5	10	17.4	6
erythritol–mannitol/EG	111.5	298.7	62.6	3	5.0	39
sebacic acid/EG	128	187.0	1.2	15	14.3	27
sebacic acid/CNT sponge	121.1	131.8	0.4		27	23
AA/EG	105.8	162.5	1.0	15	15.7	this work

[a]Supercooling degree. [b]Thermal conductivity increment of the PCC relative to that of the pure PCM.

https://dx.doi.org/10.1021/acsomega.1c00265
ACS Omega 2021, 6, 8469–8476

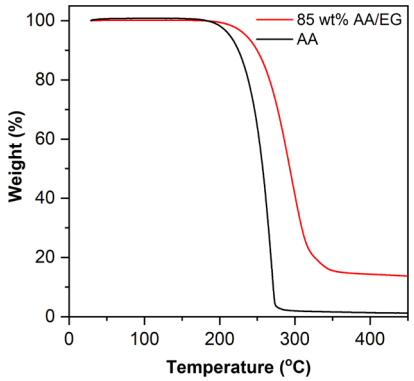

Figure 5. TGA curves of the pure AA and the 85 wt % AA/EG PCC.

PCC (~106 °C) ensured that the PCC exhibited high thermal stability during heat storage/release operations.

2.4. Cycling Durability and Chemical Stability of the AA/EG PCC. The cycling durability was evaluated based on the variations in the LHS capacity and the phase change temperature of the PCC after multiple heating/cooling cycles; thus, the long-term workability was determined. The heating/cooling cycling test was performed in an ambient atmosphere over 200 cycles using temperature-controlled oil baths (25 °C ↔ 140 °C). The LHS capacity and the phase change temperature of the PCC were determined by DSC after the cycling test. The DSC curves and the phase change properties are presented in Figure 6a and Table 1, respectively. The T_M and T_S of the as-prepared PCC were 105.8 and 104.8 °C, respectively. The T_M and T_S of the PCC after 200 cycles were 105.9 and 105.0 °C, respectively. The change in the phase change temperatures after 200 heating/cooling cycles was insignificant. The LHS capacities of the as-prepared PCC were compared with those of the PCC after the cycling test. The ΔH_M and ΔH_S of the as-prepared PCC were 162.5 and 162.2 J/g, respectively. The ΔH_M and ΔH_S of the PCC after 200 cycles were 158.4 and 158.0 J/g, respectively. The minor variation (2.6%) in the ΔH_M and ΔH_S after 200 heating/cooling cycles indicated the high durability of the AA/EG PCC. The chemical stability of the composite that was subjected to multiple thermal cycles was determined by FT-IR spectroscopy (Figure 6b). There were no significant differences in the peak positions, peak intensities, and absorption band shapes for the as-prepared and cycled composites. This indicated the high chemical stability of the PCC. It was concluded that the AA/EG PCC exhibited high cycling durability and chemical stability for long-term operations.

2.5. Thermal Conductivity of the AA/EG PCC. The thermal conductivities of the pure AA and the AA/EG PCC were determined using the transient plane source method at 25 °C (Figure 7). The pure AA exhibited a thermal conductivity

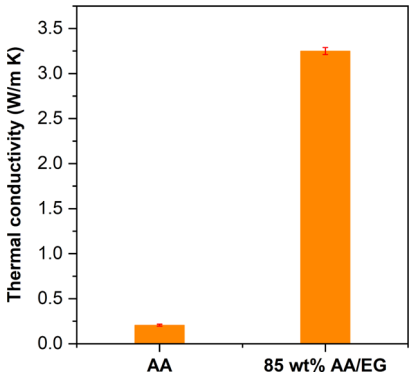

Figure 7. Thermal conductivities of the pure AA and the 85 wt % AA/EG PCC.

of 0.21 W/m·K, which was considered to be low for an organic PCM. The thermal conductivity of the PCC was 3.25 W/m·K; therefore, the thermal conductivity increased by 15.7 times as compared to that of the pure AA. This was attributed to the presence of EG with high thermal conductivity. The presence of 3−20 wt % EG increased the thermal conductivities of other EG-based PCCs (Table 2) by 5−30 times. The substantial increment (15.7 times) in the thermal conductivity of the AA/EG PCC owing to the presence of 15 wt % EG was consistent with the increment that was observed for the other studies on EG-based PCCs (refer to Table 2). The improvement in the thermal conductivity optimized the heat-transfer rate of the PCC. This resulted in the increase in the thermal performance of the PCC.

2.6. Heat Storage/Release Characteristics of the AA/EG PCC. The study of the heat storage/release characteristics is critical for the determination of the thermal performance of a PCC. The experimental setup of the heat storage/release test is shown in Figure 9, and the time-dependent variations in the temperature are presented in Figure 8. The heat storage/release properties of the PCC were superior to those of the pure AA. The results were determined using a tangential method. The PCC and the pure AA required 342 and 1702 s,

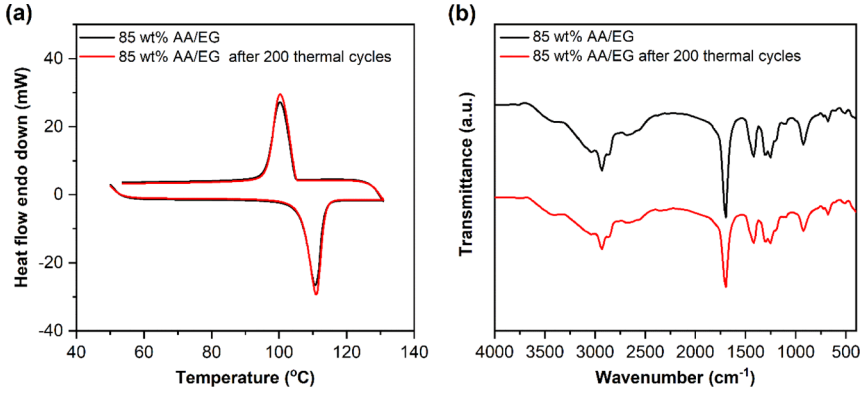

Figure 6. (a) DSC curves and (b) FT-IR spectra of the 85 wt % AA/EG PCC before and after 200 thermal cycles.

https://dx.doi.org/10.1021/acsomega.1c00265
ACS Omega 2021, 6, 8469−8476

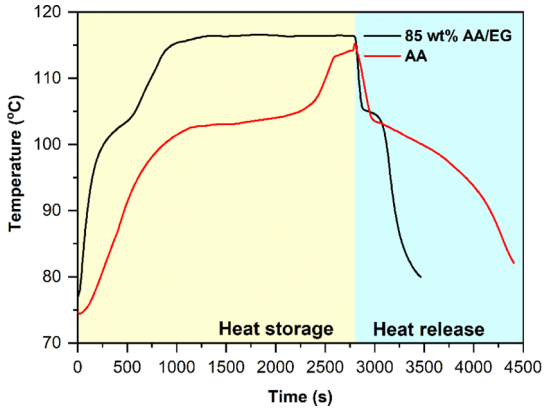

Figure 8. Heat storage/release curves showing the time-dependent temperature variation for the pure AA and the 85 wt % AA/EG PCC.

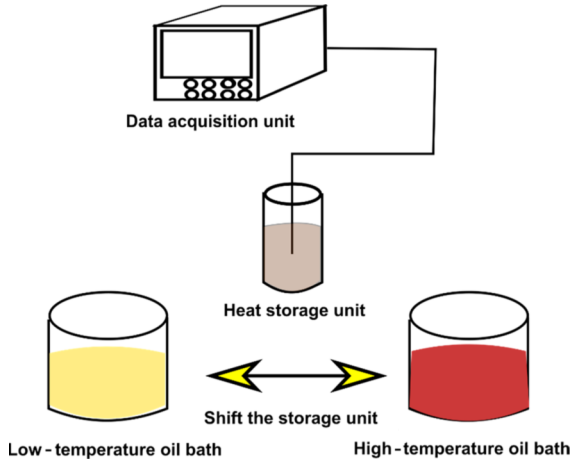

Figure 9. Schematic diagram of the setup for the heat storage/release test.

respectively, to completely melt during the heat storage. The PCC and the pure AA required 156 and 1156 s, respectively, to completely solidify during the heat release. The heat storage and release of the AA/EG PCC were 5.0-fold and 7.4-fold faster, respectively, than those of the pure AA. The composite exhibited excellent heat storage/release properties owing to its high thermal conductivity. The thermal performance of the AA/EG PCC was optimized by the fast heat storage and release.

3. CONCLUSIONS

A novel PCC, with AA as the PCM and EG as the supporting matrix, was prepared by evaporative impregnation for medium-temperature utilization. The optimal impregnation capacity of EG for AA, at which there was no leakage of liquid AA, was 85 wt %. The pure AA exhibited a ΔH_M and a ΔH_S of 202.0 and 201.2 J/g, respectively. It presented a T_M and a T_S of 108.0 and 102.2 °C, respectively, thereby resulting in a supercooling degree of 5.8 °C. The 85 wt % AA/EG PCC exhibited a ΔH_M and a ΔH_S of 162.5 and 162.2 J/g, respectively. It presented a T_M and a T_S of 105.8 and 104.8 °C, respectively, thereby resulting in a supercooling degree of only 1.0 °C. The LHS capacity and supercooling degree of the AA/EG PCC were higher and lower, respectively, than those of most of the previously studied PCCs. The thermal stability of the PCC was higher than that of the pure AA. This was attributed to the capillary forces and surface tension forces between AA and EG. Furthermore, the PCC exhibited high cycling durability and chemical stability after 200 heating/cooling cycles. The thermal conductivity of the PCC was 3.25 W/m·K; that is, it increased by 15.7 times as compared to that of the pure AA owing to the presence of EG with high thermal conductivity. The results of the heat storage/release test indicated that the heat storage and release rates of the PCC were 5.0-fold and 7.4-fold higher, respectively, than those of the pure AA. Therefore, the AA/EG PCC exhibited high potential for application as a medium-temperature heat storage medium owing to its excellent thermochemical characteristics.

4. MATERIALS AND METHODS

4.1. Materials. AA (98%) was purchased from Thermo Fisher Scientific, Massachusetts, USA. Expandable graphite was purchased from MilliporeSigma, Missouri, USA. Absolute ethanol (99%) was obtained from Samchun Chemical Co., Ltd., Seoul, South Korea.

4.2. Preparation of the AA/EG PCCs. EG was obtained by heating expandable graphite in a muffle furnace at 800−900 °C for 60 s. The AA/EG PCCs were synthesized by evaporative impregnation.[4,6] Here, 4.02, 5.69, 8.95, and 19.03 g of AA were weighed and dissolved in 200 mL of absolute ethanol. 1 g of EG was added to each solution. The mixtures were stirred at 25 °C for 2 h to obtain a uniform dispersion; thus, AA was impregnated into the pores of EG. Subsequently, the mixtures were heated to 80 °C and stirred until the complete evaporation of the solvent. The solvent was removed by heating the obtained PCCs in an oven at 130 °C for 12 h. Thus, four PCCs with different AA contents (80, 85, 90, and 95 wt %) were obtained.

4.3. Characterization Methods. The microstructures and morphologies of EG and the AA/EG PCCs were observed by field emission SEM (JSM-6701F, Jeol Ltd., Tokyo, Japan). The chemical compositions of AA, EG, and the 85 wt % AA/EG PCC were determined by FT-IR spectroscopy (Nicolet 6700, Thermo Fisher Scientific, Massachusetts, USA). The FT-IR spectra were recorded in the transmittance mode with KBr pellets over a wavenumber range of 400−4000 cm^{-1}. The crystalline phases in AA, EG, and the 85 wt % AA/EG PCC were analyzed by XRD (Miniflex, Rigaku Corporation, Tokyo, Japan). The XRD patterns were obtained using Cu Kα radiation with a current, a testing voltage, a scanning rate, and a 2θ range of 15 mA, 40 kV, 5°/min, and 5−50°, respectively.

The leakage of the materials was tested by the following procedure: first, the samples were collected on filter papers; subsequently, they were placed in an oven at 130 °C (~20 °C higher than the melting point of AA) for 60 min. Finally, the composites were removed from the filter papers and carefully observed to detect the stains of AA.

The phase change characteristics of AA and the 85 wt % AA/EG PCC were obtained by DSC (DSC 4000, PerkinElmer, Inc., Massachusetts, USA). The experiments were performed at 50−130 °C with a heating rate of 5°/min under a N_2 purge of 20 mL/min. The instrument was calibrated with standard indium and zinc before the experiments. The phase change temperatures were determined at the onset temperatures. The latent heat was obtained by integrating the area of the phase change peak. The thermal stabilities of AA and the 85 wt % AA/EG PCC were evaluated by TGA (TGA 4000, PerkinElmer, Inc., Massachusetts, USA). TGA was performed at 30−450 °C with a temperature ramp rate of 10 °C/min.

https://dx.doi.org/10.1021/acsomega.1c00265
ACS Omega 2021, 6, 8469−8476

The cycling durability of the 85 wt % AA/EG PCC was tested over 200 heating/cooling cycles. A sample (1 g) was placed in a glass vial that was subsequently cycled between two temperature-controlled oil baths (25 ↔ 140 °C). The dwell time in each bath was 5 min, which was sufficient for the tested sample to reach the temperature of the bath.

The thermal conductivity of the 85 wt % AA/EG PCC was determined using the transient plane source method (TPS 3500, Hot Disk AB, Göteborg, Sweden) at 25 °C. The measurement was performed four times for each sample to obtain an average result. The PCC was compressed into two round blocks, with each having dimensions of 30 mm × 10 mm and a weight of 5.6 g, using a homemade mold and compressor. The pure AA was melted and poured into the mold to obtain two round blocks of identical sizes; thus, the thermal conductivity was measured. The heat storage/release properties of the pure AA and the 85 wt % AA/EG PCC were investigated with a homemade apparatus (Figure 9) using the technique described in ref 40. The PCC (15 g) was compressed in a heat storage unit (30 mm × 150 mm) so that its density was as similar as those of the round blocks of the PCC in the thermal conductivity test. The pure AA (15 g) was first introduced into the heat storage unit and then melted and recrystallized prior to a heat storage/release measurement. A T-type thermocouple and a data acquisition unit (MV200, Yokogawa Electric Corporation, Tokyo, Japan) were employed to monitor the temperature changes during the tests. The heat storage unit was initially immersed in a low-temperature oil bath (75 °C) until it reached the bath temperature. Subsequently, the unit was quickly transferred to a high-temperature oil bath (120 °C), and the temperature variations during the heat storage (melting) were recorded. When the temperature of the unit reached 120 °C for a certain time, the unit was quickly transferred to the low-temperature oil bath. The temperature changes during the heat release (cooling) were monitored.

AUTHOR INFORMATION

Corresponding Author

In Park − *Research Institute of Clean Manufacturing System, Korea Institute of Industrial Technology, Cheonan 31056, South Korea; Industrial Technology, KITECH School, University of Science and Technology (UST), Daejeon 34113, South Korea;* orcid.org/0000-0002-1555-5717; Email: inpark@kitech.re.kr

Authors

Giang Tien Nguyen − *Research Institute of Clean Manufacturing System, Korea Institute of Industrial Technology, Cheonan 31056, South Korea; Industrial Technology, KITECH School, University of Science and Technology (UST), Daejeon 34113, South Korea*

Ha Soo Hwang − *Research Institute of Clean Manufacturing System, Korea Institute of Industrial Technology, Cheonan 31056, South Korea; R&D Center, OomphChem Inc., Cheonan 31080, South Korea*

Jiyoung Lee − *Research Institute of Clean Manufacturing System, Korea Institute of Industrial Technology, Cheonan 31056, South Korea; Department of Chemical and Biomolecular Engineering, Yonsei University, Seoul 09722, South Korea*

Complete contact information is available at: https://pubs.acs.org/10.1021/acsomega.1c00265

Notes

The authors declare no competing financial interest.

ACKNOWLEDGMENTS

This research was financially supported by the Ministry of Trade, Industry and Energy (Republic of Korea) through Korea Evaluation Institute of Industrial Technology (KEIT) (no. 20011253).

REFERENCES

(1) Fallahi, A.; Guldentops, G.; Tao, M.; Granados-Focil, S.; Van Dessel, S. Review on solid-solid phase change materials for thermal energy storage: Molecular structure and thermal properties. *Appl. Therm. Eng.* **2017**, *127*, 1427−1441.

(2) Pielichowska, K.; Pielichowski, K. Phase change materials for thermal energy storage. *Prog. Mater. Sci.* **2014**, *65*, 67−123.

(3) Shukla, A.; Buddhi, D.; Sawhney, R. L. Solar water heaters with phase change material thermal energy storage medium: A review. *Renew. Sustain. Energy Rev.* **2009**, *13*, 2119−2125.

(4) Li, Z.; Wu, Z.-G. Development of medium-temperature composite phase change material with high thermal stability and conductivity. *Sol. Energy Mater. Sol. Cells* **2016**, *155*, 341−347.

(5) Kenisarin, M. M. High-temperature phase change materials for thermal energy storage. *Renew. Sustain. Energy Rev.* **2010**, *14*, 955−970.

(6) Yuan, M.; Ren, Y.; Xu, C.; Ye, F.; Du, X. Characterization and stability study of a form-stable erythritol/expanded graphite composite phase change material for thermal energy storage. *Renew. Energy* **2019**, *136*, 211−222.

(7) Pintaldi, S.; Perfumo, C.; Sethuvenkatraman, S.; White, S.; Rosengarten, G. A review of thermal energy storage technologies and control approaches for solar cooling. *Renew. Sustain. Energy Rev.* **2015**, *41*, 975−995.

(8) Ren, Y.; Xu, C.; Yuan, M.; Ye, F.; Ju, X.; Du, X. $Ca(NO_3)_2$-$NaNO_3$/expanded graphite composite as a novel shape-stable phase change material for mid- to high-temperature thermal energy storage. *Energy Convers. Manag.* **2018**, *163*, 50−58.

(9) Zhou, C.; Wu, S. Medium- and high-temperature latent heat thermal energy storage: Material database, system review, and corrosivity assessment. *Int. J. Energy Res.* **2019**, *43*, 621−661.

(10) del Barrio, E. P.; Godin, A.; Duquesne, M.; Daranlot, J.; Jolly, J.; Alshaer, W.; Kouadio, T.; Sommier, A. Characterization of different sugar alcohols as phase change materials for thermal energy storage applications. *Sol. Energy Mater. Sol. Cells* **2017**, *159*, 560−569.

(11) Solé, A.; Neumann, H.; Niedermaier, S.; Martorell, I.; Schossig, P.; Cabeza, L. F. Stability of sugar alcohols as PCM for thermal energy storage. *Sol. Energy Mater. Sol. Cells* **2014**, *126*, 125−134.

(12) Gil, A.; Oró, E.; Miró, L.; Peiró, G.; Ruiz, Á.; Salmerón, J. M.; Cabeza, L. F. Experimental analysis of hydroquinone used as phase change material (PCM) to be applied in solar cooling refrigeration. *Int. J. Refrig.* **2014**, *39*, 95−103.

(13) Seki, Y.; İnce, Ş.; Ezan, M. A.; Turgut, A.; Erek, A. Graphite nanoplates loading into eutectic mixture of Adipic acid and Sebacic acid as phase change material. *Sol. Energy Mater. Sol. Cells* **2015**, *140*, 457−463.

(14) Haillot, D.; Bauer, T.; Kröner, U.; Tamme, R. Thermal analysis of phase change materials in the temperature range 120−150°C. *Thermochim. Acta* **2011**, *513*, 49−59.

(15) Paul, A.; Shi, L.; Bielawski, C. W. A eutectic mixture of galactitol and mannitol as a phase change material for latent heat storage. *Energy Convers. Manag.* **2015**, *103*, 139−146.

(16) Oró, E.; de Gracia, A.; Castell, A.; Farid, M. M.; Cabeza, L. F. Review on phase change materials (PCMs) for cold thermal energy storage applications. *Appl. Energy* **2012**, *99*, 513−533.

(17) Tang, J.; Yang, M.; Yu, F.; Chen, X.; Tan, L.; Wang, G. 1-Octadecanol@hierarchical porous polymer composite as a novel shape-stability phase change material for latent heat thermal energy storage. *Appl. Energy* **2017**, *187*, 514−522.

https://dx.doi.org/10.1021/acsomega.1c00265
ACS Omega 2021, 6, 8469−8476

(18) Xiao, Q.; Yuan, W.; Li, L.; Xu, T. Fabrication and characteristics of composite phase change material based on $Ba(OH)_2 \cdot 8H_2O$ for thermal energy storage. *Sol. Energy Mater. Sol. Cells* **2018**, *179*, 339−345.
(19) Sarı, A.; Karaipekli, A. Preparation, thermal properties and thermal reliability of palmitic acid/expanded graphite composite as form-stable PCM for thermal energy storage. *Sol. Energy Mater. Sol. Cells* **2009**, *93*, 571−576.
(20) Sun, K.; Kou, Y.; Zheng, H.; Liu, X.; Tan, Z.; Shi, Q. Using silicagel industrial wastes to synthesize polyethylene glycol/silica-hydroxyl form-stable phase change materials for thermal energy storage applications. *Sol. Energy Mater. Sol. Cells* **2018**, *178*, 139−145.
(21) Wang, Y.; Xia, T. D.; Zheng, H.; Feng, H. X. Stearic acid/silica fume composite as form-stable phase change material for thermal energy storage. *Energy Build.* **2011**, *43*, 2365−2370.
(22) Xiao, X.; Zhang, P.; Li, M. Experimental and numerical study of heat transfer performance of nitrate/expanded graphite composite PCM for solar energy storage. *Energy Convers. Manag.* **2015**, *105*, 272−284.
(23) Zhang, Q.; Liu, J. Sebacic acid/CNT sponge phase change material with excellent thermal conductivity and photo-thermal performance. *Sol. Energy Mater. Sol. Cells* **2018**, *179*, 217−222.
(24) Fu, L.; Wang, Q.; Ye, R.; Fang, X.; Zhang, Z. A calcium chloride hexahydrate/expanded perlite composite with good heat storage and insulation properties for building energy conservation. *Renew. Energy* **2017**, *114*, 733−743.
(25) Chung, O.; Jeong, S.-G.; Kim, S. Preparation of energy efficient paraffinic PCMs/expanded vermiculite and perlite composites for energy saving in buildings. *Sol. Energy Mater. Sol. Cells* **2015**, *137*, 107−112.
(26) Xia, L.; Zhang, P.; Wang, R. Z. Preparation and thermal characterization of expanded graphite/paraffin composite phase change material. *Carbon* **2010**, *48*, 2538−2548.
(27) Wang, S.; Qin, P.; Fang, X.; Zhang, Z.; Wang, S.; Liu, X. A novel sebacic acid/expanded graphite composite phase change material for solar thermal medium-temperature applications. *Sol. Energy* **2014**, *99*, 283−290.
(28) Gasco, M. R.; Gallarate, M.; Pattarino, F. In vitro permeation of azelaic acid from viscosized microemulsions. *Int. J. Pharm.* **1991**, *69*, 193−196.
(29) Hojabri, L.; Kong, X.; Narine, S. S. Fatty Acid-Derived Diisocyanate and Biobased Polyurethane Produced from Vegetable Oil: Synthesis, Polymerization, and Characterization. *Biomacromolecules* **2009**, *10*, 884−891.
(30) Lane, G. A.; Goldstein, A. N. Dibasic acid based phase change material compositions. U.S. Patent 5755988 A, May 26, 1998.
(31) Zhang, D.; Chen, M.; Wu, S.; Liu, Q.; Wan, J. Preparation of expanded graphite/polyethylene glycol composite phase change material for thermoregulation of asphalt binder. *Constr. Build. Mater.* **2018**, *169*, 513−521.
(32) Li, Y.; Yan, H.; Wang, Q.; Wang, H.; Huang, Y. Structure and thermal properties of decanoic acid/expanded graphite composite phase change materials. *J. Therm. Anal. Calorim.* **2017**, *128*, 1313−1326.
(33) Zhao, M.; Liu, P. Adsorption of methylene blue from aqueous solutions by modified expanded graphite powder. *Desalination* **2009**, *249*, 331−336.
(34) Goudarzi, R.; Hashemi Motlagh, G. The effect of graphite intercalated compound particle size and exfoliation temperature on porosity and macromolecular diffusion in expanded graphite. *Heliyon* **2019**, *5*, No. e02595.
(35) Thalladi, V. R.; Nüsse, M.; Boese, R. The Melting Point Alternation in α,ω-Alkanedicarboxylic Acids. *J. Am. Chem. Soc.* **2000**, *122*, 9227−9236.
(36) Park, I.; Peng, H.-g.; Gidley, D. W.; Xue, S.; Pinnavaia, T. J. Epoxy−Silica Mesocomposites with Enhanced Tensile Properties and Oxygen Permeability. *Chem. Mater.* **2006**, *18*, 650−656.
(37) Xia, L.; Zhang, P. Thermal property measurement and heat transfer analysis of acetamide and acetamide/expanded graphite composite phase change material for solar heat storage. *Sol. Energy Mater. Sol. Cells* **2011**, *95*, 2246−2254.
(38) Jiang, Z.; Leng, G.; Ye, F.; Ge, Z.; Liu, C.; Wang, L.; Huang, Y.; Ding, Y. Form-stable $LiNO_3-NaNO_3-KNO_3-Ca(NO_3)_2$/calcium silicate composite phase change material (PCM) for mid-low temperature thermal energy storage. *Energy Convers. Manag.* **2015**, *106*, 165−172.
(39) Zeng, J.-L.; Chen, Y.-H.; Shu, L.; Yu, L.-P.; Zhu, L.; Song, L.-B.; Cao, Z.; Sun, L.-X. Preparation and thermal properties of exfoliated graphite/erythritol/mannitol eutectic composite as form-stable phase change material for thermal energy storage. *Sol. Energy Mater. Sol. Cells* **2018**, *178*, 84−90.
(40) Lv, P.; Liu, C.; Rao, Z. Experiment study on the thermal properties of paraffin/kaolin thermal energy storage form-stable phase change materials. *Appl. Energy* **2016**, *182*, 475−487.

https://dx.doi.org/10.1021/acsomega.1c00265
ACS Omega 2021, 6, 8469−8476